Sound radiation from a resilient spherical cap on a rigid sphere

Ronald M. Aarts[a)] and Augustus J.E.M. Janssen
Philips Research Europe
HTC 36 (WO-02)
NL-5656AE Eindhoven
The Netherlands

(Dated: January 8, 2010)

It has been argued that the sound radiation of a loudspeaker is modeled realistically by assuming the loudspeaker cabinet to be a rigid sphere with a resilient spherical cap. Series expansions, valid in the whole space outside the sphere, for the pressure due to a harmonically excited cap with an axially symmetric velocity distribution are presented. The velocity profile is expanded in functions orthogonal on the cap rather than on the whole sphere. As a result only a few expansion coefficients are sufficient to accurately describe the velocity profile. An adaptation of the standard solution of the Helmholtz equation to this particular parametrization is required. This is achieved by using recent results on argument scaling of orthogonal (Zernike) polynomials. The approach is illustrated by calculating the pressure due to certain velocity profiles that vanish at the rim of the cap to a desired degree. The associated inverse problem, in which the velocity profile is estimated from pressure measurements around the sphere, is also feasible as the number of expansion coefficients to be estimated is limited. This is demonstrated with a simulation.

PACS numbers: 43.38 Ar, 43.20 Bi, 43.20 Px, 43.40 At
Keywords: loudspeaker, loudspeaker characterization, Helmholtz equation with spherical boundary conditions, resilient pole cap sound radiation, Legendre polynomial, Zernike expansion, scaling Zernike polynomials

I. INTRODUCTION

The sound radiation of a loudspeaker is quite often modeled by assuming the loudspeaker cabinet to be a rigid infinite baffle around a circularly symmetric membrane. Given a velocity distribution on the membrane, the pressure in front of the baffle due to a harmonic excitation is then described by the Rayleigh integral[1] or by King's integral[2]. These integrals have given rise to an impressive arsenal of analytic results and numerical methods for the pressure and other acoustical quantities in journal papers[3–17] and textbooks[18–24]. The results thus obtained are in good correspondence with what one finds, numerically or otherwise, when the loudspeaker is modeled as being a finite-extent box-like cabinet with a circular, vibrating membrane. Here one should limit attention to the region in front of the loudspeaker and not too far from the axis through the middle of and perpendicular to the membrane. The validity of the infinite-baffle model becomes questionable, or even nonsensical, on the side region or behind the loudspeaker[22] (p. 181). An alternative model, with potential for more adequately dealing with the latter regions, assumes the loudspeaker to be a rigid sphere equipped with a membrane in a spherical cap of the sphere. It has been argued by Morse and Ingard[20] (Sec. 7.2), that using the sphere as a simplified model of a loudspeaker whose cabinet has roughly the same width, height and depth, produces comparable acoustical results as the true loudspeaker (also see Fig. 2 of the present paper). An application for the cap model is that it can be used to predict the polar behavior of a loudspeaker cabinet. Modeling the loudspeaker as a resilient spherical cap on a rigid sphere would have the attractive feature that the solution of the Helmholtz equation for the pressure is feasible as a series involving the spherical harmonics and spherical Hankel functions, see Ref.18 (Ch. 11.3), Ref.19 (Ch. III, Sec. 6), Ref.20 (Ch. 7) and Ref.21 (Chs. 19–20), and expansion coefficients to be determined from the boundary condition at the sphere (including the resilient cap).

In the present paper, the velocity profile is assumed to be axially symmetric but otherwise general. It was shown by Frankort[25] that this is a realistic assumption for loudspeakers, because their cones mainly vibrate in a radially symmetric fashion. These loudspeaker velocity profiles can be parameterized conveniently and efficiently in terms of expansion coefficients relative to functions orthogonal on the cap. The orthogonal functions used are the Zernike terms $R_{2\ell}^0$, as occur in Ref.16, 17 for the case of a resilient circular radiator in an infinite baffle, to which an appropriate variable transformation is applied so as to account for the geometry of the cap. A formula will be developed that expresses the required coefficients in the standard solution of the Helmholtz equation in terms of the Zernike expansion coefficients of the velocity profile on the cap. This then gives rise to a formula, explicitly in terms of these Zernike coefficients, for the pressure at any point on and outside the sphere. As examples of the resulting forward computation scheme, profiles of the Stenzel type (certain type of smooth functions of the elevation angle that vanish at the rim of the cap to any desired degree) are considered. The correspond-

[a)]Ronald.M.Aarts@philips.com; Also at Technical University Eindhoven, Den Dolech 2, PT3.23, P.O Box 513, NL-5600 MB Eindhoven, The Netherlands

ing inverse problem, in which the expansion coefficients of the unknown profile are estimated from the measured pressure that the profile gives rise to, is also feasible. This is largely due to the fact that the expansion terms are orthogonal and complete so that for smooth velocity profiles only a few coefficients are required. Thus, for such velocity profiles, the profile can be readily estimated from pressure measurements around the sphere.

In Ref.16, 17 a similar approach has been used for radiation from a circular radiator in an infinite baffle. A special Zernike expansion of the exponential factor occurring in the Rayleigh integral for the pressure yields in Ref.16 an explicit formula for the on-axis pressure in terms of the Zernike coefficients of the velocity profile on the radiator. This formula is used for forward computation of the on-axis pressure as well as for solving the inverse problem of estimating the velocity profile through its Zernike coefficients from measured on-axis pressure data. Furthermore, the 0^{th} order Hankel transform of the Zernike terms have a particular simple form in terms of Bessel functions of the first kind. In Ref.16 this is used to express the far-field pressure explicitly in terms of the Zernike coefficients of the velocity profile on the radiator. In Ref.17 a similar thing is done, via King's integral expression for the pressure, to find series expansions for acoustical quantities such as the pressure at the edge of the radiator, the radiator force on the radiator, the radiated power and the directivity.

The results and methods in the present paper differ from those in the previous literature[18–21] and from those in Ref.16, 17 in the following manner. In Refs.18–21 the attention is restricted to the case of a velocity profile with constant radial or axial component. In this paper, general axially symmetric profiles are allowed. Next, the pressure in the whole space in and outside the sphere (and not just on the axis or in the far field) is computed. This gives naturally rise to expressions for the on-axis and for the far-field pressure as in Ref.16, and to expressions for the acoustical quantities, as considered in Ref.17, for the case of radiation from a spherical cap on a spherical baffle. Due to the different geometry than the one used in Ref.16, 17, a variable transformation is required to pass from orthogonal functions on the disk to orthogonal functions on the cap. Furthermore, the expansion coefficients required in the solution of the Helmholtz equation must be expressed in terms of the expansion coefficients of the velocity profile on the cap. This is achieved here by using a recent explicit result[26,27] on variable-scaling of Zernike terms, a result that has not been used previously in the acoustical setting.

The results in this paper are of a (semi-)analytical nature which distinguish these from the ones obtained by more numerically oriented method, such as in Ref.28 and in Ref.29. In Ref.28 a boundary element method (BEM) is used to predict acoustical radiation from axisymmetric surfaces with arbitrary boundary conditions, and in Ref.29 near-field acoustical holography (NAH) is used to characterize acoustical radiators from near-field pressure data. While these methods are powerful tools for the forward and inverse problem, the analytic approach with a simplified model can yield additional insights as to the role of the various parameters and expansion coefficients. In particular, in the forward method, the influence on the pressure and related quantities of a particular Zernike term in the expansion of the velocity profile is reflected directly in terms of the involved expansion coefficient of which quite often only a few are needed. Furthermore, the inverse method can also be used for design purposes in which one has to match a desired, rather than a measured, pressure distribution in the field.

II. BASIC FORMULAS AND OVERVIEW

Assume a general velocity profile $V(\theta,\varphi)$ on a spherical cap, given in spherical coordinates as

$$S_0 = \{(r,\theta,\varphi) \mid r = R\,,\ 0 \le \theta \le \theta_0\,,\ 0 \le \varphi \le 2\pi\}\ , \quad (1)$$

with R the radius of the sphere with center at the origin and θ_0 the angle between the $z-$axis (elevation angle $\theta = 0$) and any line passing through the origin and a point on the rim of the cap. See Fig. 1 for the geometry and the notations used in this paper. Thus it is assumed

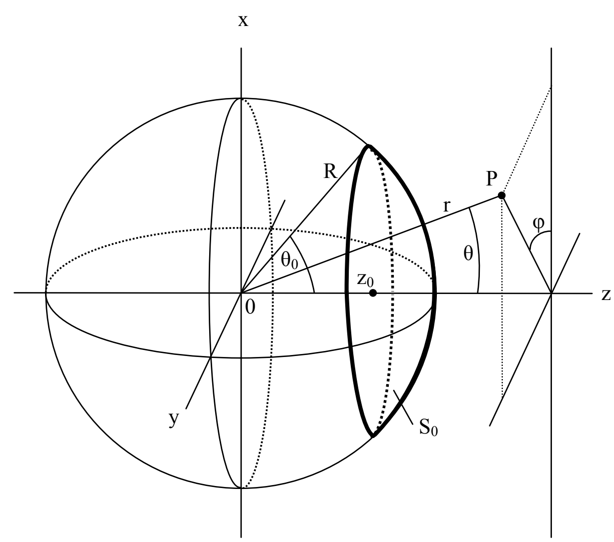

FIG. 1. Geometry and notations. The area outlined with the thick curves is the cap denoted by S_0.

that V vanishes outside S_0. Furthermore, in loudspeaker applications, the cap moves parallel to the z-axis, and so $V(\theta,\varphi)$ will be identified with its z-component, and has normal component

$$W(\theta,\varphi) = V(\theta,\varphi)\cos\theta\ . \quad (2)$$

The average of this normal component over the cap,

$$\frac{1}{A_{S_0}} \iint\limits_{S_0} W(\theta,\varphi)\sin\theta\, d\theta\, d\varphi\ , \quad (3)$$

is denoted by w_0, where A_{S_0} is the area of the cap, see Eq. (10). Then the time-independent part $p(r,\theta,\varphi)$ of the pressure due to a harmonic excitation of the membrane is given by

$$p(r,\theta,\varphi) = \\ -i\rho_0 c \sum_{n=-\infty}^{\infty} \sum_{m=-n}^{n} W_{mn}\, P_n^{|m|}(\cos\theta)\, \frac{h_n^{(2)}(kr)}{h_n^{(2)'}(kR)} e^{im\varphi} \ , \tag{4}$$

see Ref.20 (Ch. 7) or Ref.21 (Ch. 19) (Helmholtz equation with spherical boundary conditions). Here ρ_0 is the density of the medium, c is the speed of sound in the medium, $k = \omega/c$ is the wave number and ω is the radial frequency of the applied excitation, and $r \geq R$, $0 \leq \theta \leq \pi$, $0 \leq \varphi \leq 2\pi$. Furthermore, $P_n^{|m|}(\cos\theta)e^{im\varphi}$ is the spherical harmonic Y_n^m in exponential notation (compare with Ref.20 (Sec. 7.2), where sine-cosine notation has been used), $h_n^{(2)}$ is the spherical Hankel function, see Ref.30 (Ch. 10), of order n, and W_{mn} are the expansion coefficients of $W(\theta,\varphi)$, $0 \leq \theta \leq \pi$, $0 \leq \varphi \leq 2\pi$, relative to the basis $Y_n^m(\theta,\varphi)$. Thus

$$W_{mn} = \frac{n+1/2}{2\pi} \frac{(n-|m|)!}{(n+|m|)!} \\ \int_0^{\pi}\int_0^{2\pi} W(\theta,\varphi)\, P_n^{|m|}(\cos\theta) e^{-im\varphi} \sin\theta \, d\theta \, d\varphi \ , \tag{5}$$

where it should be observed that the integration over θ in Eq. (5) is in effect only over $0 \leq \theta \leq \theta_0$ since V vanishes outside S_0.

In the case of axially symmetric velocity profiles V and W, written as $V(\theta)$ and $W(\theta)$, the Eqs. (4) and (5) become independent on φ and simplify to

$$p(r,\theta,\varphi) = -i\rho_0 c \sum_{n=0}^{\infty} W_n\, P_n(\cos\theta)\, \frac{h_n^{(2)}(kr)}{h_n^{(2)'}(kR)} \ , \tag{6}$$

and

$$W_n = (n+1/2) \int_0^{\pi} W(\theta)\, P_n(\cos\theta) \sin\theta \, d\theta \ , \tag{7}$$

respectively, with P_n the Legendre polynomial of degree n. The integration in Eq. (7) is actually over $0 \leq \theta \leq \theta_0$. Since loudspeakers mainly vibrate in a radially symmetric fashion, almost all attention in this paper is limited to axially symmetric velocity profiles V and W. In Sec. VI the generalization to non-axial symmetric profiles is briefly considered.

The case that W is constant w_0 on the cap S_0 has been treated in Ref.19 (Part III, Sec. 6), Ref.20 (p. 343), and Ref.21 (Sec. 20.5), with the result that

$$W_n = \frac{1}{2} w_0 (P_{n-1}(\cos\theta_0) - P_{n+1}(\cos\theta_0)) \ . \tag{8}$$

The pressure p is then obtained by inserting W_n into Eq. (6). Similarly, the case that V is constant v_0 on S_0 has been treated by Ref.21 (Sec. 20.6), with the result that

$$W_n = \tfrac{1}{2} v_0 \{ \tfrac{n+1}{2n+3} (P_n(\cos\theta_0) - P_{n+2}(\cos\theta_0)) + \\ \tfrac{n}{2n-1} (P_{n-2}(\cos\theta_0) - P_n(\cos\theta_0)) \} \ . \tag{9}$$

In Eqs. (8) and (9) the definition $P_{-n-1} = P_n$, $n = 0,1,\cdots$, has been used to deal with the case $n = 0$ in Eq. (8) and the cases $n = 0,1$ in Eq. (9). In Fig. 2 the resemblance is shown between the polar plots of: a real driver in a rectangular cabinet (Fig. 2-a), a rigid piston in an infinite baffle (Fig. 2-b), and a rigid spherical cap in a rigid sphere (Fig. 2-c) using Eqs. (6) and (9). The driver (Vifa MG10SD09-08, $a = 3.2$ cm) was mounted in a square side of a rectangular cabinet with dimensions 13x13x18.6 cm and measured on a turning table in an anechoic room at 1 m distance. Figure 2 clearly shows that the resemblance between polar plots of the measured loudspeaker (a), and those of the sphere model (c) is much better than the often used infinite baffle model (b). In particular, at low frequencies the (solid) curve in (b) is independent of the angle, which is not the case for (a) and (c). At higher frequencies the overall shape and in particular the notches of (b) does not exhibit the resemblance such as between (a) and (c). Finally, for angles between 90° an 270° the infinite baffle model (b) is nonsensical. The area of the spherical cap is equal to

$$A_{S_0} = 4\pi R^2 \sin^2(\theta_0/2). \tag{10}$$

If this area is chosen to be equal to the area of the flat piston, there follows for the piston radius

$$a = 2R\sin(\theta_0/2). \tag{11}$$

The parameters used for Fig. 2 are $a = 3.2$ cm, $\theta_0 = \pi/8$, $R = 8.2$ cm, are such—using Eq. (11)—that the area of the piston and the cap are equal. The radius R of the sphere is such that the sphere and cabinet have comparable volumes, respectively 2.3 and 3.1 liter. If R is such that the sphere volume is the same as that of the cabinet, and θ_0 such that the area of the piston and the cap are equal, one gets $R = 9.0873$ cm and $\theta_0 = 0.35399$ rad (≈20°). The corresponding polar plot—Fig. 2-d—is very similar to Fig. 2-c, the deviations are about 1 dB or less. Apparently, the actual value of the volume is of modest influence.

It should be noted that the W_n in Eqs. (8) and (9) have slow decay, roughly like $n^{-1/2}$ (see Eq. (B5) in Appendix B), and this shows that the representation of W through its Legendre coefficients is highly inefficient. While slow decay of W_n in Eq. (6) is not necessarily a problem for the forward problem (where the pressure p is computed from W using Eqs. (6) and (7)), it certainly is for the inverse problem. In the inverse problem, one aims at estimating the velocity profile W (or V) from pressure measurements around the sphere. This can be done, in principle, by adopting a matching approach in Eq. (6) in which the W_n are optimized with respect to match of the measured pressure p and the theoretical expression for p in Eq. (6) involving the W_n. Already for the simplest case that W is constant, it is seen from the slow decay of the W_n and the slow decay of $P_n(\cos\theta)$ that a very large number of terms are required in the Legendre series $W(\theta) = \sum_{n=0}^{\infty} W_n P_n(\cos\theta)$.

In this paper a more efficient representation of W is employed. This representation uses orthogonal functions on the cap that are derived from Zernike terms

$$R_{2\ell}^0(\rho) = P_\ell(2\rho^2 - 1) \ , \ 0 \leq \rho \leq 1 \ , \ \ell = 0,1,\cdots \ , \tag{12}$$

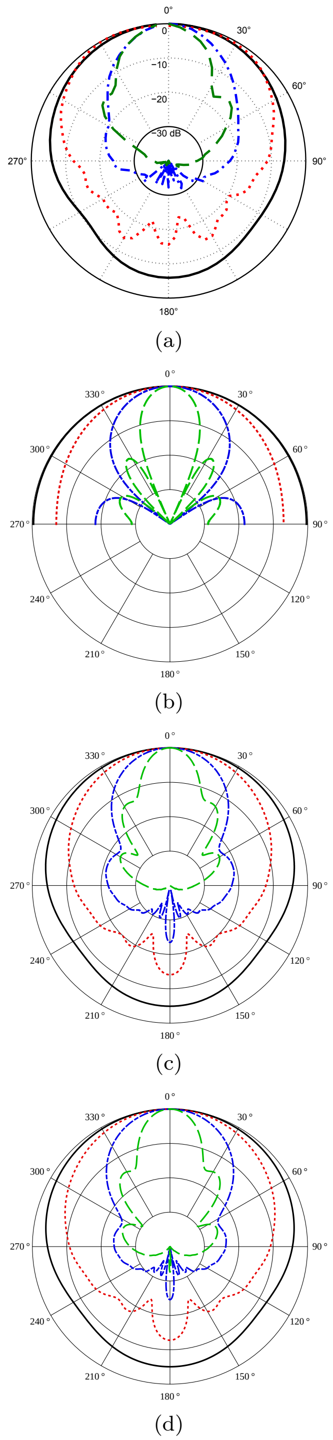

FIG. 2. (Color online) Polar plots of the SPL (10 dB/div.), f= 1 kHz (solid curve), 4 kHz (dotted curve), 8 kHz (dashed-dotted curve), and 16 kHz (dashed curve), corresponding for $c = 340$ m/s and $a = 3.2$ cm to ka values: 0.591, 2.365, 4.731, 9.462. (a) Loudspeaker (radius $a = 3.2$ cm, measuring distance $r = 1$ m) in rectangular cabinet. (b) Rigid piston ($a = 3.2$ cm) in infinite baffle. (c) Rigid spherical cap (aperture $\theta_0 = \pi/8$, sphere radius $R = 8.2$ cm, $r = 1$ m) using Eqs. (6) and (9). The parameters a, R, and θ_0 are such—using Eq. (11)—that the area of the piston and the cap are equal. (d) same as (c) but with a sphere volume equal to that of the cabinet, and $R = 9.0873$ cm and $\theta_0 = 0.35399$ rad. All curves are normalized such that the SPL is 0 dB at θ=0.

that were also used in Ref.16, 17. These Zernike terms arise uniquely when the set of radially symmetric functions $\rho^{2j} = (x^2+y^2)^j$, $j = 0, 1, \cdots$, on the unit disk $x^2 + y^2 \le 1$ are orthogonalized with respect to the inner product

$$\iint\limits_{x^2+y^2\le 1} A(x,y)B^*(x,y)dxdy \qquad (13)$$

for function A and B on the unit disk (also see Eq. (27) and the text below Eq. (27)). Thus

$$\frac{1}{\pi}\iint\limits_{x^2+y^2\le 1} R^0_{2\ell}((x^2+y^2)^{1/2})R^0_{2k}((x^2+y^2)^{1/2})dxdy$$

$$= 2\int_0^1 R^0_{2\ell}(\rho)R^0_{2k}(\rho)\rho d\rho = \frac{\delta_{\ell k}}{2\ell+1} \; . \qquad (14)$$

Because of the geometry of the spherical cap, a variable transformation is required to pass from orthogonal function $R^0_{2\ell}$ on the disk to orthogonal functions on the cap. This is achieved by setting

$$C^0_{2\ell}(\theta) = R^0_{2\ell}\left(\frac{\sin\frac{1}{2}\theta}{\sin\frac{1}{2}\theta_0}\right) \; , \; 0 \le \theta \le \theta_0 \; , \qquad (15)$$

for $\ell = 0, 1, \cdots$, see Appendix A. With

$$\theta = 2\arcsin(s_0\rho) \; ; s_0 = \sin\frac{1}{2}\theta_0 \; , \qquad (16)$$

the inverse of the variable transformation used in Eq. (15), it holds by completeness and orthogonality of the Zernike terms that

$$W(2\arcsin(s_0\rho)) = w_0\sum_{\ell=0}^{\infty} u_\ell R^0_{2\ell}(\rho) \; , \; 0 \le \rho \le 1 \; , \qquad (17)$$

where the expansion coefficients $w_0 u_\ell$ are given by

$$w_0 u_\ell = 2(2\ell+1)\int_0^1 W(2\arcsin(s_0\rho))R^0_{2\ell}(\rho)d\rho \; . \qquad (18)$$

It is this parametrization of W in terms of the expansion coefficients u_ℓ that will be preferred in the sequel. This parametrization is obtained by "warping" W according to Eq. (16) and expanding the resulting warped function as in Eqs. (17)–(18), with s_0 given in Eq. (16).

The efficiency of the representation in Eq. (17) is apparent from the fact that a smooth profile W requires only a limited number terms with coefficients u_ℓ of relatively small amplitude in Eq. (17) to yield an accurate approximation of $W(2\arcsin(s_0\rho))$. For instance, the constant profile $W = w_0$ on S_0 is represented exactly by only one such term, $w_0 R^0_0(\rho)$, in the expansion in Eq. (17), and the profile $W = v_0\cos\theta$, corresponding to the case that V is constant v_0 on S_0, is represented exactly by two terms

$v_0[(1-s_0^2)R_0^0(\rho)-s_0^2R_2^0(\rho)]$. More complicated examples arise when V or W is a multiple of the Stenzel profile

$$(n+1)\Big(\frac{\cos\theta-\cos\theta_0}{1-\cos\theta_0}\Big)^n\ , \tag{19}$$

and these require $n+1$ terms in the representation in Eq. (17). These profiles vanish at the rim of S_0 to degree n and are considered in Sec. V and VI to illustrate the methods developed in this paper.

In Sec. III it will be shown that the expansion in Eq. (17) gives rise to the formula

$$W_n=(-1)^n s_0 w_0\sum_{\ell=0}^{n}(R_{2n+1}^{2\ell+1}(s_0)-R_{2n-1}^{2\ell+1}(s_0))u_\ell\ , \tag{20}$$

expressing the coefficients W_n required in Eq. (6) for the pressure in terms of the expansion coefficients u_ℓ in Eq. (17). From this a series expansion for the pressure p in the whole space $r\geq R$, $\theta\in[0,\pi]$ and $\varphi\in[0,2\pi]$ follows as

$$p(r,\theta,\varphi)=-i\rho_0 c w_0\sum_{\ell=0}^{\infty}u_\ell S_\ell(r,\theta)\ , \tag{21}$$

where

$$S_\ell(r,\theta)=\sum_{n=\ell}^{\infty}(-1)^n s_0(R_{2n+1}^{2\ell+1}(s_0)-R_{2n-1}^{2\ell+1}(s_0))P_n(\cos\theta)\frac{h_n^{(2)}(kr)}{h_n^{(2)'}(kR)}\ , \tag{22}$$

in which

$$R_n^m(\rho)=\rho^m P_{\frac{n-m}{2}}^{(0,m)}(2\rho^2-1)\ , \tag{23}$$

for integer $n,m\geq 0$ with $n-m$ even and ≥ 0 ($R_n^m\equiv 0$ otherwise) with $P_k^{(\alpha,\beta)}(x)$ the general Jacobi polynomial[30]. The functions

$$A_{nm}(x,y)=R_n^{|m|}(\rho)\,\mathrm{e}^{im\alpha}\ ,\ x=\rho\cos\alpha\ ,\ y=\rho\sin\alpha\ , \tag{24}$$

are known in optics[31,32] as the circle polynomials of Zernike and they have been introduced recently in acoustics as well[16,17]. They have been shown by Bhatia and Wolf[31] to arise uniquely as orthogonal functions, see Eq. (13), that satisfy form invariance under rotations of the unit disk.

The main result in Eqs. (20)–(23) provides the generalization of the forward computation scheme in Eqs. (6), (8), (9) to general axially symmetric velocity profiles W. Furthermore, it provides the basis for the inverse problem, in which the expansion coefficients u_ℓ are estimated from measured pressure data around the sphere by adopting a best match approach in Eq. (21). From these estimated coefficients an estimate of W can be made on basis of Eq. (17).

In Sec. IV the forward computation scheme embodied by the Eqs. (21)–(23) is discussed in some detail. It is shown how the results in Eqs.(8)–(9) arise for the two special cases considered there, and the matter of convergence of the series in Eq. (22) and some computational issues are addressed. In Sec. V the forward method is exemplified for the case that V or W is a Stenzel-type profile, see Eq. (19). In Sec. VI the inverse method is illustrated in simulation. In Sec. VII the extension of the methodology to non-axial symmetric profiles is briefly discussed. In Sec. VIII the results of this paper are discussed, applications of these to audio engineering phenomena and quantities are considered, and some issues for future investigations are mentioned. The conclusions are presented in Sec. IX. Finally, in Appendix A the orthogonality of the functions $C_{2\ell}^0$ in Eq. (15) is established, in Appendix B, the asymptotics of the terms in the series for S_ℓ in Eq. (22) as $n\to\infty$ is given which is required for the convergence matter in Sec. IV, and in Appendix C the R_n^m are given in the form of a Discrete Cosine Transform which allows fast and reliable computation of the Zernike terms of large degree.

III. DERIVATION OF THE MAIN RESULT

In this section the main result of Eqs. (20)–(23) on the coefficients W_n required in the solution of the Helmholtz equation and the pressure p due to an axially symmetric, radial velocity component $W(\theta)$ vanishing outside the spherical cap S_0 is proved. Our initial aim is to show Eq. (28) that expresses W_n in terms of $W(\theta)$, warped according to Eqs. (16) and (17), and the scaled Zernike terms $R_{2n}^0(s_0\rho)$. Then a result from the scaling theory of Zernike terms is used to establish Eq. (20) and, subsequently, Eqs. (22) and (23). Thus from Eq. (7) and the substitutions $\mu=\cos\theta$, $\mu=2y^2-1$ it follows that

$$\begin{aligned}W_n&=(n+1/2)\int_0^{\theta_0}W(\theta)P_n(\cos\theta)\sin\theta\,d\theta=\\ &4(n+1/2)\int_{\cos\frac12\theta_0}^1 W(\arccos(2y^2-1))P_n(2y^2-1)y\,dy\ .\end{aligned} \tag{25}$$

Next, the substitution $y=\sqrt{1-x^2}$ is made, and it is used that

$$P_n(-z)=(-1)^n P_n(z),\ \arccos(1-2x^2)=2\arcsin x\ . \tag{26}$$

This gives

$$W_n=2(2n+1)(-1)^n\int_0^{s_0}W(2\arcsin x)P_n(2x^2-1)x\,dx\ , \tag{27}$$

where $s_0=\sin\frac12\theta_0$ as in Eq. (16). Next, the definition $R_{2n}^0(x)=P_n(2x^2-1)$, see Eq. (12), is used, the substitution $x=s_0\rho$ with $0\leq\rho\leq 1$ is made, and it follows that

$$\begin{aligned}W_n&=2(2n+1)(-1)^n s_0^2\cdot\\ &\int_0^1 W(2\arcsin(s_0\rho))R_{2n}^0(s_0\rho)\rho\,d\rho\ .\end{aligned} \tag{28}$$

Now there is the following general result[26,27] on argument scaling of the polynomials R_s^r, see Eq. (23):

$$R_s^r(\epsilon\rho)=\sum_t\frac{t+1}{s+1}\,\frac{1}{\epsilon}(R_{s+1}^{t+1}(\epsilon)-R_{s-1}^{t+1}(\epsilon))R_t^r(\rho)\ . \tag{29}$$

Here r and s are integers ≥ 0 with $s-r$ even and ≥ 0 (recall that $R_n^m = 0$ when $n < m$) and t in the summation in Eq. (29) assumes the values $r, r+2, \cdots, s$; ϵ and ρ are arbitrary ≥ 0. Using this result with

$$r = 0\,,\ s = 2n\,,\ \epsilon = s_0\,,\ \rho = \rho \qquad (30)$$

in Eq. (28), together with Eq. (18), it follows that

$$W_n = (-1)^n s_0 w_0 \sum_{\ell=0}^{n} (R_{2n+1}^{2\ell+1}(s_0) - R_{2n-1}^{2\ell+1}(s_0)) u_\ell\ . \quad (31)$$

This is Eq. (20). Then Eq. (21) for p, with S_ℓ given by Eq. (22), follows upon inserting the result of Eq. (31) for W_n into Eq. (6) and interchanging the summations over n and ℓ.

IV. DISCUSSION OF THE MAIN RESULT

In this section the main result in Eqs. (20)–(23) is discussed in some detail. It is shown how the special cases of constant W or constant V on the cap arise, see Eqs. (6)–(9). Furthermore, the order of magnitude of the terms in the series for S_ℓ in Eqs. (22) as $n \to \infty$ is indicated. The latter analysis shows that, especially when r is not large compared to R, many terms n are required. In Sec. IV.C it is proposed to compute (high-degree) Zernike polynomials by employing their representation in Eq. (23) in terms of Jacobi polynomials where the latter are computed using Mathematica. An alternative method, based on an expression for $R_n^m(\rho)$, using the Discrete Cosine Transform, is presented in Appendix C.

A. Special case $W = w_0$ on S_0

The result in Eq. (8) for the special case that W is constant w_0 on S_0 does not immediately follow from Eq. (20). As already noted, $u_0 = 1$, $u_1 = u_2 = \cdots = 0$ in this case. Due to the various recurrence relations[30] that exist for the Jacobi polynomials, the result in Eq. (20) can be brought into a variety of different forms. As one of these, there holds for $n = 1, 2, \cdots$

$$\begin{aligned} &2s_0(R_{2n+1}^1(s_0) - R_{2n-1}^1(s_0)) = \\ &R_{2n+2}^0(s_0) - R_{2n-2}^0(s_0))\ , \end{aligned} \qquad (32)$$

and the Eq. (8) for W_n follows using that, see Eq. (12),

$$\begin{aligned} &R_{2k}^0(s_0) = P_k(2\sin^2 \tfrac{1}{2}\theta_0 - 1) = \\ &P_k(-\cos\theta) = (-1)^k P_k(\cos\theta)\ . \end{aligned} \qquad (33)$$

In principle, recursion techniques can also be used to establish the result in Eq. (9) for W_n in the case that V is constant v_0 on S_0.

B. Special case W is a simple source on S_0

If the polar cap aperture θ_0 is decreasing, in the limit the cap will act as a simple source. Using Eqs. (21)–(23) and by proper normalization by the cap area A_{S_0}, using Eq. (10), and the definition of w_0 by Eq. (3), there holds

$$p(r,\theta,\varphi) = -i\rho_0 c w_0 \sum_{n=0}^{\infty} (2n+1) P_n(\cos\theta)\, \frac{h_n^{(2)}(kr)}{h_n^{(2)'}(kR)}\ . \qquad (34)$$

In Fig. 3 the corresponding polar plot is illustrated, where the same sphere radius and frequencies are used as in Fig. 2-c.

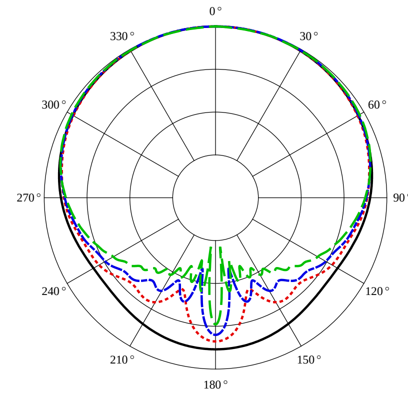

FIG. 3. (Color online) Polar plots of the SPL (10 dB/div.) of a simple source on a sphere of radius R =0.082 m. Frequency $f = 1$ kHz (solid curve), 4 kHz (dotted curve), 8 kHz (dashed-dotted curve), and 16 kHz (dashed curve), at distance r = 1 m, using Eqs. (34). All curves are normalized such that the SPL is 0 dB at θ=0.

C. Convergence analysis of the series S_ℓ and computational aspects

As already said, for smooth velocity profiles W only a limited number of coefficients u_ℓ in the expansion in Eq. (17) have to be considered. In Appendix B it is shown that the terms

$$s_0(R_{2n+1}^{2\ell+1}(s_0) - R_{2n-1}^{2\ell+1}(s_0)) P_n(\cos\theta) \frac{h_n^{(2)}(kr)}{h_n^{(2)'}(kR)} \qquad (35)$$

in the series defining S_ℓ in Eq. (22) are of the order of magnitude

$$\frac{kR}{(n+1)^{3/2}} \Big(\frac{R}{r}\Big)^{n+1} \text{and}\ \frac{kR}{(n+1)^2} \Big(\frac{R}{r}\Big)^{n+1}\ , \qquad (36)$$

respectively, when θ is near 0 or π and away from 0 and π, respectively. Here it is assumed that θ_0 is not close to 0 or π. The estimate of the order of magnitude is accurate when ℓ is fixed and n exceeds $\frac{1}{4}(kr)^2$. It then follows from the analysis in Ref.33 (Sec. 5) that the truncation error after the N^{th} term in the series of Eq. (22) for S_ℓ has order of magnitude $kN^{-1/2}(R/r)^N$ and $kN^{-1}(R/r)^N$, respectively, for the corresponding θ-ranges. Hence, when r is allowed to approach R, a relatively large number of terms is required in the series for S_ℓ.

Implementation of Eqs. (21) and (22) requires computation of the quantity in Eq. (35), normally for low or moderate values of ℓ and possibly for large values of n. These computations have been done for the present paper in Mathematica. The Zernike polynomials and Legendre polynomials occurring in Eqs. (35) can be expressed in terms of Jacobi polynomials $P_j^{(\alpha,\beta)}$, see Eqs. (12) and (23), and Mathematica computes these polynomials, virtually without any restrictions to the values of the parameters α and β or to the degree j, provided that a sufficient precision has been set. If this is not applicable then the method discussed in Appendix C might be useful because Eq. (C2) is very robust against precision problems. Next, $h_n^{(2)}(kr)$ and $h_n^{(2)'}(kR)$ must be computed. Now $h_n^{(2)'}$ can be expressed in terms of $h_n^{(2)}$, $h_{n\pm1}^{(2)}$, see Ref.30, Eqs. 10.1.19–22, and the evaluation of the $h^{(2)}$-functions can be done in Mathematica, virtually without any restriction to the order j and argument z of $h_j^{(2)}(z)$. Finally, $h_n^{(2)'}(kR)$ occurs in the numerator in Eq. (35), and for this it should be checked that $h_n^{(2)'}$ has no real zeros. By Ref.30, Eq. 10.1.6,

$$W\{j_n(z),y_n(z)\} = j_n(z)y_n'(z) - j_n'(z)y_n(z) = \frac{1}{z^2} \quad (37)$$

and by Ref.30, Subsec. 10.1.1,

$$h_n^{(2)'}(z) = j_n'(z) - iy_n'(z) \quad (38)$$

in which $j_n'(z)$ and $y_n'(z)$ are real for real z. Hence,

$$|h_n^{(2)'}(z)|^2 = |j_n'(z)|^2 + |y_n'(z)|^2 \geq \frac{1}{|z|^4(|j_n(z)|^2 + |y_n(z)|^2)} \ , \quad (39)$$

showing that $h_n^{(2)'}(z)$ is bounded away from 0.

V. STENZEL-TYPE PROFILES AND FORWARD COMPUTATION

Consider the profile

$$V^{(K)}(\theta) = v_0^{(K)}(K+1)\Big(\frac{\cos\theta - \cos\theta_0}{1-\cos\theta_0}\Big)^K \ , \ 0 \leq \theta \leq \theta_0 \ , \quad (40)$$

with $V^{(K)}(\theta) = 0$ for $\theta_0 < \theta \leq \pi$ (as usual), $K = 0, 1, \cdots$. Then a simple computation shows that

$$V^{(K)}(2\arcsin(s_0\rho)) = v_0^{(K)}(K+1)(1-\rho^2)^K \ , 0 \leq \rho \leq 1 \ . \quad (41)$$

The right-hand side of Eq. (41) is the Stenzel profile, considered extensively in Ref.16. Thus

$$V^{(K)}(2\arcsin(s_0\rho)) = v_0^{(K)} \sum_{\ell=0}^{K} q_\ell^{(K)} R_{2\ell}^0(\rho) \ , \ 0 \leq \rho \leq 1 \ , \quad (42)$$

where

$$q_\ell^{(K)} = (K+1)(-1)^\ell \, \frac{2\ell+1}{\ell+1} \, \frac{\binom{K}{\ell}}{\binom{K+\ell+1}{K}} \ , \ \ell = 0, 1, \cdots, K \ . \quad (43)$$

From

$$W^{(K)}(\theta) = V^{(K)}(\theta)\cos\theta = \frac{K+1}{K+2}(1-\cos\theta_0)V^{(K+1)}(\theta) + (\cos\theta_0)V^{(K)}(\theta) \ , \quad (44)$$

it follows that

$$W^{(K)}(2\arcsin(s_0\rho)) = w_0^{(K)} \sum_{\ell=0}^{K+1} u_\ell^{(K)} R_{2\ell}^0(\rho) \ , \ 0 \leq \rho \leq 1 \ , \quad (45)$$

where

$$w_0^{(K)} = \frac{K+1+\cos\theta_0}{K+2} v_0^{(K)} \ , \quad (46)$$

and, for $\ell = 0, 1, \cdots, K+1$,

$$u_\ell^{(K)} = \frac{v_0^{(K)}}{w_0^{(K)}} \big[\tfrac{K+1}{K+2}(1-\cos\theta_0)q_\ell^{(K+1)} + (\cos\theta_0)q_\ell^{(K)}\big]. \quad (47)$$

Thus one can compute the pressure using the formulas in Eqs. (21)–(23) with $u_\ell = u_\ell^{(K)}$.

In Fig. 4 polar plots are displayed of the SPL (10 dB/div.) of a spherical cap ($\theta_0 = \pi/8$, $R = 8.2$ cm, $r = 1$ m) with various Stenzel velocity profiles, K=0 (solid curve), K=1 (dotted curve), K=2 (dashed-dotted curve), and K=3 (dashed curve), (a) f = 4 kHz, (b) f = 8 kHz. It appears that the difference between the various velocity profiles are more pronounced at higher frequencies. Also, the cap becomes less directive for higher K values because in the limit $K \to \infty$ it would behave like a simple source on a sphere. Furthermore, it appears that the solid curves ($K = 0$) for (a) f = 4 kHz and (b) f = 8 kHz are the same as the dotted and dashed-dotted curves, respectively in Fig. 2-c, while different formulas were involved.

VI. INVERSE PROBLEM

The Eqs. (21)–(23) show how to compute the pressure in the space $r \geq R$ due to a harmonically excited (wave number k) membrane on the spherical cap $0 \leq \theta \leq \theta_0$ with a known radial component W of a velocity profile. In the reverse direction, the Eqs. (21)–(23) can serve as the basis for a method for estimating W from measurements of the pressure p in the space $r \geq R$ that W gives rise to. Such a profile W can usually be estimated accurately by a limited number of expansion coefficients u_ℓ in Eq. (17), and these can be estimated by taking a matching approach in Eq. (22) in which the u_ℓ are chosen such that they optimize the match between the measured pressure and the theoretical expression involving the u_ℓ at the right-hand side of Eq. (22). Given measurements, see Fig. 1,

$$\hat{p_j} = \hat{p_j}(P_j) \ , P_j = r_j(\cos\varphi_j\sin\theta_j, \sin\varphi_j\sin\theta_j, \cos\theta_j) \ , \quad (48)$$

where $j = 0, 1, \cdots, J$, the numbers $d_\ell, \ell = 0, 1, \cdots, L$, are chosen such that

$$\sum_{j=0}^{J} |\hat{p}_j - \sum_{\ell=0}^{L} d_\ell S_\ell(r_j,\theta_j)|^2 \sin\theta_j \ , \quad (49)$$

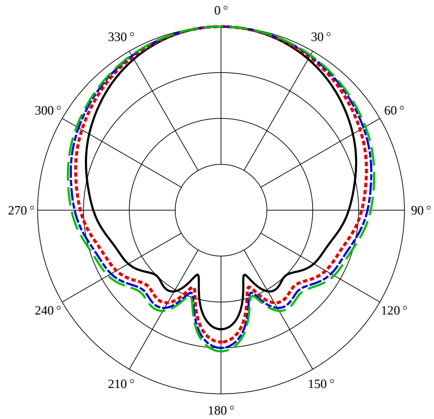

(a)

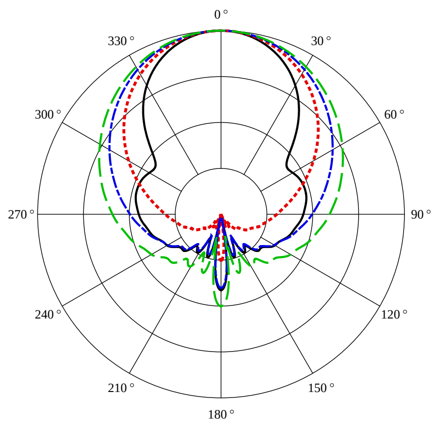

(b)

FIG. 4. (Color online) Polar plots of the SPL (10 dB/div.) of a spherical cap ($\theta_0 = \pi/8$, $R = 8.2$ cm, $r = 1$ m) with various Stenzel velocity profiles, K=0 (solid curve), K=1 (dotted curve), K=2 (dashed-dotted curve), and K=3 (dashed curve). (a) f = 4 kHz, (b) f = 8 kHz. All curves are normalized such that the SPL is 0 dB at θ=0.

is minimal. The solution of this minimization problem can be obtained by using 'Solve' of Mathematica, or by other means. Then $w_0\,, u_\ell\,, \ell = 0, 1, \cdots, L$ are estimated by setting

$$d_0 = -i\rho_0 c w_0\ , u_\ell = d_\ell / d_0\ ,\ \ell = 0, 1, \cdots, L\,. \tag{50}$$

There are various questions that arise in connection with the above optimization problem, such as number and choice of the measurement points P_j, choice of L, condition of the linear systems that occur, influence of noise and of systematic errors (such as incorrect setting of R and/or θ_0), etc. It is out of the scope of the present paper to address any of these issues in detail. Instead, just one simulation example is given.

Simulation example

Take $R = 8.2$ cm, $\theta_0 = \pi/4$, $k = \omega/c = 2\pi f/c$ with $c =$ 340 m/s, f= 4 kHz, so that $kR = 6$. The measurement points $P_j(r_j, \theta_j, \varphi_j)$ are taken in the form

$$R\,2^{j_1/J_1} = r(j_1)\ ,\ \frac{\pi(j_2 - \frac{1}{2})}{J_2} = \theta(j_2)\ ,\ \frac{2\pi(j_3 - \frac{1}{2})}{J_3} = \varphi(j_3)\ , \tag{51}$$

with $j_1 = 1, \cdots, J_1 = 4$, $j_2 = 1, \cdots, J_2 = 6$, $j_3 = 1, \cdots, J_3 = 6$. Such a set of measurement points yields a convenient implementation of the solution of the optimization problem but does not need to be optimal in any other respect (matters as optimal choice of the measurement points are outside the scope of this paper). The profile W is chosen to be

$$W^{(K)}(\theta) = V^{(K)}(\theta)\cos\theta\ ,\ 0 \le \theta \le \theta_0\ , \tag{52}$$

where $V^{(K)}(\theta)$ is the $K^{\rm th}$ Stenzel-type profile as in Sec. V (see Eqs. (40), (44)), and $K = 2$. We require for this example $v_0 = v_0^{(K)} = 1$ m/s, and by Eqs. (46) and (47) we get respectively $w_0 = w_0^{(K)}$ and

$$u_\ell^{(K)} = \tfrac{K+2}{K+1+\cos\theta_0}\left[\tfrac{K+1}{K+2}(1-\cos\theta_0)q_\ell^{(K+1)} + (\cos\theta_0)q_\ell^{(K)}\right]. \tag{53}$$

Using $q_\ell^{(K+1)}$, $q_\ell^{(K)}$ given by Eq. (43), the pressure p is computed in accordance with Eq. (21) with $u_\ell = u_\ell^{(K)}$. Measurements $\hat{p}_j$ are obtained in simulation by adding complex white noise (by adding scaled random numbers by Mathematica's 'RandomComplex[-1 - I, 1 + I, Length[p]]' where the scaling is such that the SNR becomes 40 dB) to the computed $p(P_j)$. The non-zero coefficients of $W^{(K)}$ are estimated by taking $L = K + 1$ in the optimization problem, and this yields estimates $\hat{w}_0$, $\hat{u}_0, \cdots, \hat{u}_{K+1}$ of $w_0, u_0, \cdots, u_{K+1}$. Figure 5 shows the input profile $W^{(K)}$ of Eq. (52) using Eq. (40) directly (solid curve) together with the reconstructed profiles

$$\hat{W}^{(K)}(\theta) = \hat{w}_0^{(K)} \sum_{\ell=0}^{K+1} \hat{u}_\ell R_{2\ell}^0\Big(\frac{\sin\frac{1}{2}\theta}{\sin\frac{1}{2}\theta_0}\Big)\ ,\ 0 \le \theta \le \theta_0\ , \tag{54}$$

without noise (dotted curve) and with noise (dashed-dotted curve) added to the pressure points $\hat{p}_j$. The recovered $\hat{u}_\ell$ are computed by solving Eq. (49) and using Eqs. (50), (45), and s_0 from (16). Figure 5 shows that the (noiseless) reconstructed profile (dotted curve) coincides with the input profile (solid curve), and that the recovered profile using the noisy pressure points (dashed-dotted curve) is very similar to the other two curves. The method appears to be robust for noise contamination. Figure 6 shows the pressure points at various angles and distances vs. index i, using Eq. (51) and $i = j_3 + (j_2 - 1)J_3 + (j_1 - 1)J_2 J_3$, with the pressure points $|p_i|$ without noise (filled circles), pressure points $|\hat{p}_i|$ with noise (squares), and recovered pressure points (45° rotated squares). Note that the noiseless and recovered pressure points are nearly coincident, which again shows that the method appears to be robust for noise contamination. Figure 7 shows the corresponding polar plot of the velocity profile of Fig. 5. The solid curve in Fig. 7 is for the near field ($r = 0.0975$ m) and the dotted curve for the far field ($r = 1$ m).

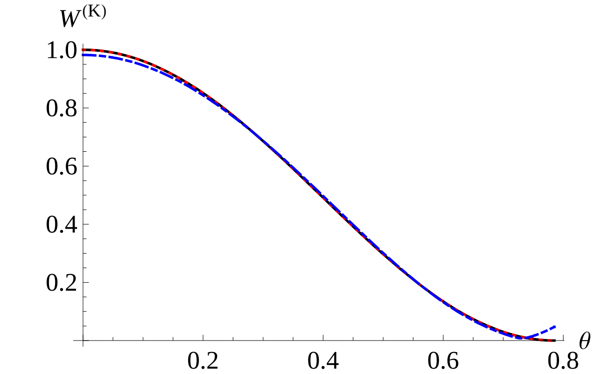

FIG. 5. (Color online) Input profile $W^{(K)}/(K+1)$ ($K=2$ and $\theta_0=\pi/4$) of Eq. (52) using Eq. (40) directly (solid curve) together with the reconstructed profiles $\hat{W}^{(K)}$ without noise (dotted curve) and with noise added to the pressure points $\hat{p}_j$ (dashed-dotted curve). The (noiseless) reconstructed profile (dotted curve) coincides with the input profile (solid curve).

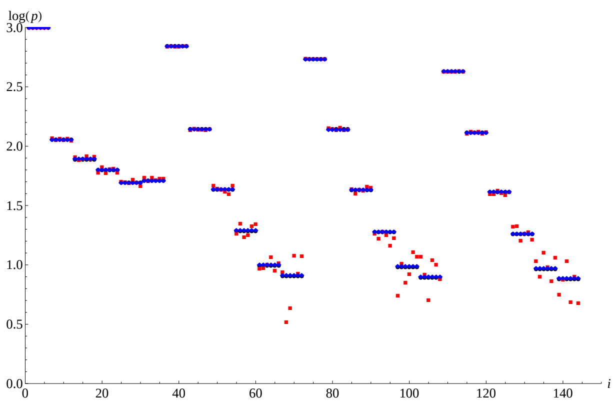

(a)

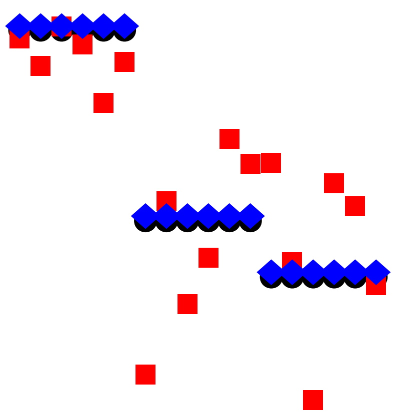

(b)

FIG. 6. (Color online) (a) Pressure points at various angles and distances vs. index i, using Eq. (51) and $i=j_3+(j_2-1)J_3+(j_1-1)J_2J_3$, with the pressure points $|p_i|$ without noise (filled circles), pressure points $|\hat{p}_i|$ with noise (squares), and recovered pressure points (45° rotated squares). The noiseless and recovered pressure points are nearly coincident. (b) enlarged portion of (a) from $90\le i\le 110$, and $0.6\le\log(|p|)\le 1.3$

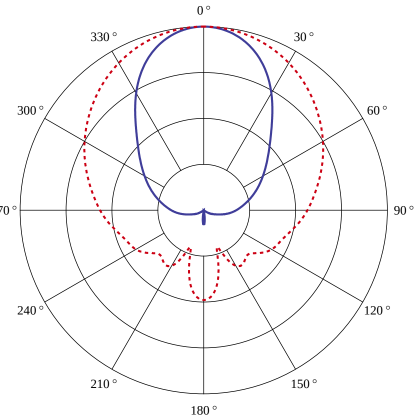

FIG. 7. (Color online) Polar plots (10 dB/div.) in the near field (solid curve, $r=0.0975$ m) and in the far field (dotted curve, $r=1$ m), corresponding to the parameters of the simulation example and the velocity profile of Fig. 5. All curves are normalized such that the SPL is 0 dB at θ=0.

VII. EXTENSION TO NON-AXIALLY SYMMETRIC PROFILES

Loudspeaker membranes vibrate mainly in a radially symmetric fashion, in particular at low frequencies. At higher frequencies, break-up behavior can occur, and then it may be necessary to consider non-radially symmetric profiles. In the present context, where a loudspeaker is modeled as consisting of a rigid spherical cabinet with a resilient spherical cap, this requires consideration of non-axially symmetric velocity profiles $V(\theta,\varphi)$ and $W(\theta,\varphi)$ on S_0. Thus, the general formula in Eq. (5) has to be considered now. The methodology of this paper is extended to this situation by considering the expansion on the disk $0\le\rho\le 1$, $0\le\varphi\le 2\pi$,

$$\begin{aligned}&W(2\arcsin(s_0\rho,\varphi)) =\\ &w_0\sum_{m=-\infty}^{\infty}\sum_{s=0}^{\infty}a_{|m|+2s}^{|m|}R_{|m|+2s}^{|m|}(\rho)e^{im\varphi}\ ,\end{aligned}\tag{55}$$

with the general polynomials $R_n^m(\rho)$ given by Eq. (23). This then leads to a series expansion for the pressure p of the form

$$\begin{aligned}&p(r,\theta,\varphi)) =\\ &-i\rho c w_0\sum_{m=-\infty}^{\infty}\sum_{s=0}^{\infty}a_{|m|+2s}^{|m|}T_{ms}(r,\theta,\varphi)\ ,\end{aligned}\tag{56}$$

where

$$T_{ms}(r,\theta,\varphi)=\sum_{n=|m|}^{\infty}Q_{mns}P_n^{|m|}(\cos\theta)\frac{h_n^{(2)}(kr)}{h_n^{(2)'}(kR)}\ ,\tag{57}$$

and where the quantities Q_{mns} are to be discussed below. The formula in Eq. (56) can be used for forward computation, when the profile W and its expansion coefficients $a_{|m|+2s}^m$ are known, as well as for solving the inverse problem in which the profile W is estimated via its expansion coefficients from measured pressure data around the sphere $r = R$.

The Q_{mns} in Eq. (57) are obtained by inserting the expansion in Eq. (55) into the integral expression in Eq. (5) for W_{mn}. Upon integration over φ, this yields

$$Q_{mns} = 4(n+1/2)s_0^2 \tfrac{(n-|m|)!}{(n+|m|)!} J_{ns}^{|m|} \ , \tag{58}$$

where

$$J_{ns}^{|m|} = \int_0^1 P_n^{|m|}(1-2s_0^2\rho^2) R_{|m|+2s}^{|m|}(\rho)\rho \, d\rho \ . \tag{59}$$

The evaluation of the J-integrals is still feasible in semi-analytic form using the general scaling result in Eq. (29), but is quite a bit more complicated than in the case that $m = 0$. This is due to the fact that $P_n^m(1-2x^2)$ is given by the complicated expression

$$P_n^m(1-2x^2) = \tfrac{(n+m)!}{n!} x^m (1-x^2)^{m/2} P_{n-m}^{(m,m)}(1-2x^2) \ , \tag{60}$$

with $P_j^{(\alpha,\beta)}$ the general Jacobi polynomials. Therefore, the evaluation of the $J_{ns}^{|m|}$ as $R_{|m|+2s}^{|m|}$-coefficients of the function $P_n^{|m|}(1-2s_0^2\rho^2)$ requires dedicated results from the theory of polynomial expansions. This is outside the scope of the present paper.

VIII. DISCUSSION AND OUTLOOK

In this paper the foundation is laid for a method to perform forward and inverse sound pressure computations for a spherical cap on an otherwise rigid sphere with a non-uniform velocity profile. This method naturally applies to spherically shaped loudspeakers, but it appears that even non-spherical loudspeakers with a cone shaped driver have polar responses that resemble quite well the polar responses produced by the spherical model for frequencies from low frequencies to well over 10 kHz. Thus the spherical model can be used more generally to predict loudspeaker behavior and for loudspeaker design purposes. In the forward problem, the velocity profile is assumed to be known and the sound pressure is expressed in the whole space on and outside the sphere as a series involving the special functions S_ℓ of Eq. (22), with coefficients u_ℓ the expansion coefficients of the velocity profile warped as in Eq. (16) and (17). This yields a versatile tool, both for the forward problem of computing p from the velocity profile and for the inverse problem. In the inverse problem, the velocity profile is unknown and is estimated in terms of Zernike expansion coefficients from pressure data measured around the sphere by adopting a matching approach based on the series solution just mentioned for the pressure. Well-behaved velocity profiles are already adequately represented by only a few terms of their Zernike expansion. Therefore, the Zernike series approach is convenient for both the forward problems and the inverse problem.

The inverse procedure has not been fully worked out in the present paper due to a variety of practical issues that need to be addressed. Among these practical issues are

- choice of the measurement points,
- condition of the linear systems that arise,
- influence of wave number k, radius R and aperture angle $2\theta_0$,
- influence of noise,
- influence of misalignment of the measurement points, for instance, due to wrong choice of origin,
- influence of inclination of the axis,
- incorrect setting of the radius of the radiator,

while various combinations of these issues should also be considered. The authors intend to work out the method for the loudspeaker assessment with attention for the above mentioned points.

In the present paper we have considered only the pressure in the field. However, having the required field point pressure in analytical form, various acoustical quantities become available in an analytical form. In investigations that are carried out presently, a remarkable resemblance is seen between measured quantities—like baffle-step response, sound power, directivity, and acoustic center—from the loudspeaker of Fig. 2-a and the corresponding quantities computed using the spherical model.

There are presently available numerical methods that can be used both for the forward problem, for instance, Boundary Element Methods (BEM)[28], and for the inverse problem, for instance, Near-field Acoustic Holography (NAH)[29]. These methods can be deployed in case of general geometries and yield the pressure with arbitrary accuracy. However, for a general understanding and to get a feeling for the influence of the various parameters on both the pressure and associated quantities, the availability of a simple analytic, in certain respects adequate model, as the one that we have here, is of complementary value.

IX. CONCLUSIONS

Appropriately warped Legendre polynomials provide an efficient and robust method to describe velocity profiles of a resilient spherical cap on a rigid sphere. Only a few coefficients are necessary to approximate various velocity profiles, in particular Stenzel profiles. The polar plot of a rigid spherical cap on a rigid sphere is already quite similar to that of a real loudspeaker, and is useful in the full 4π-field. The spherical-cap model yields polar plots that exhibit good full range similarity with the polar plots from real loudspeakers. It thus outperforms the more conventional model in which the loudspeaker is modeled as a rigid piston in an infinite baffle. The cap model can be used to predict the polar behavior of a loudspeaker cabinet. The presented method enables one to solve the inverse problem of calculating the actual velocity profile of the cap radiator using (measured) on- and off-axis sound pressure data. This computed velocity profile allows the extrapolation to far-field loudspeaker pressure data, including off-axis behavior.

Acknowledgments

The authors wish to thank Okke Ouweltjes for assisting in the loudspeaker measurements and making the plot for Fig. 2a, and Prof. Fred Simons for providing pertinent assistance in programming Mathematica, in particular to make Fig. 5.

APPENDIX A: ORTHOGONALITY OF $C_{2\ell}^0$

From the definition in Eq. (15) and orthogonality of the $R_{2\ell}^0$ as in Eq. (14) it follows that

$$\int_0^{\theta_0} C_{2\ell}^0(\theta) C_{2k}^0(\theta) \sin\theta \, d\theta =$$
$$4 \int_0^{\theta_0} R_{2\ell}^0\Big(\frac{\sin\frac{1}{2}\theta}{\sin\frac{1}{2}\theta_0}\Big) R_{2k}^0\Big(\frac{\sin\frac{1}{2}\theta}{\sin\frac{1}{2}\theta_0}\Big) \sin\frac{1}{2}\theta \, d(\sin\frac{1}{2}\theta) =$$
$$\frac{2\delta_{\ell k}}{2\ell+1} s_0^2 \; . \tag{A1}$$

Here $s_0 = \sin\frac{1}{2}\theta_0$ as in Eq. (16) and the substitution $\rho = s_0^{-1}\sin\frac{1}{2}\theta$ has been used so that Eq. (14) can be applied.

APPENDIX B: LARGE n BEHAVIOR OF THE TERMS IN EQ.(36)

The large-n behavior of the terms in Eq. (35) is determined by the large-n behavior of the three factors

$$s_0\big(R_{2n+1}^{2\ell+1}(s_0) - R_{2n-1}^{2\ell+1}(s_0)\big) \, , \; P_n(\cos\theta) \, , \; \frac{h_n^{(2)}(kr)}{h_n^{(2)'}(kR)} \; . \tag{B1}$$

Here $s_0 = \sin\frac{1}{2}\theta_0$, $r \geq R$, and ℓ is assumed to be fixed.

It follows from the definition of R_n^m in Eq. (23) and Ref.34 (Thm. 8.21.12) that

$$\begin{aligned} & s_0\big(R_{2n+1}^{2\ell+1}(s_0) - R_{2n-1}^{2\ell+1}(s_0)\big) = \\ & (-1)^{n-\ell}(\tfrac{1}{2}\theta_0 \tan\tfrac{1}{2}\theta_0)^{1/2} \cdot \\ & \{\delta_{n+1} J_{2\ell+1}((n+1)\theta_0) + \delta_n J_{2\ell+1}(n\theta)\} \end{aligned} \tag{B2}$$

with absolute error of the order $\theta_0^{1/2} n^{-3/2}$. Here $J_{2\ell+1}$ is the Bessel function of the first kind and of order $2\ell+1$, and $0 \leq \delta_n, \ \delta_{n+1} \leq 1$. It is assumed here that $\theta_0 \in (0,\pi)$ is not close to π. When θ_0 is also not close to 0, it follows from the asymptotics of $J_{2\ell+1}(z)$ as $z \to \infty$, see Ref.30 (Ch. 9) that

$$s_0(R_{2n+1}^{2\ell+1}(s_0) - R_{2n-1}^{2\ell+1}(s_0)) = \mathrm{O}(\frac{1}{\sqrt{n+1}}) \tag{B3}$$

as $n \to \infty$, with constant implied by the O-symbol of order unity.

Next, by Ref.34 (Thm. 8.21.6)

$$P_n(\cos\theta) = \Big(\frac{\theta}{\sin\theta}\Big)^{1/2} J_0((n+1/2)\theta) \tag{B4}$$

as $n \to \infty$, with absolute error of the order $\theta^{1/2} n^{-3/2}$. Here $\theta \in (0,\pi)$ is not close to π. Using that $P_n(\cos(\pi-\theta)) = (-1)^n P_n(\cos\theta)$, it is concluded from $|J_0(z)| \leq 1$ and the asymptotics of $J_0(z)$ as $z \to \infty$, see Ref.30 (Ch. 9), that

$$P_n(\cos\theta) = \mathrm{O}(1) \text{ and } \mathrm{O}(\frac{1}{\sqrt{n+1}}) \tag{B5}$$

as $n \to \infty$ and where $\theta \in [0,\pi]$ is arbitrary and $\theta \in (0,\pi)$ is away from 0 and π, respectively. The constants implied by the O-symbols in Eq. (B5) are of the order unity.

Finally, from Ref.30 (Ch. 10),

$$\begin{aligned} h_n^{(2)}(z) &= i\,\tfrac{1\cdot 3\cdot \cdots \cdot(2n-1)}{z^{n+1}} \, , \\ h_n^{(2)'}(z) &= -(n+1)i\,\tfrac{1\cdot 3\cdot \cdots \cdot(2n-1)}{z^{n+2}} \end{aligned} \tag{B6}$$

as $n \to \infty$, with relative errors of the order $z^2/4n$. Thus

$$\frac{h_n^{(2)}(kr)}{h_n^{(2)'}(kR)} = \frac{-kR}{n+1}\Big(\frac{R}{r}\Big)^{n+1} \tag{B7}$$

as $n \to \infty$, with relative error of the order $(kr)^2/4n$ when $r \geq R$.

From Eqs. (B3), (B5) and (B7) the claims on the order of magnitude of the terms in Eq. (35) for large n and fixed ℓ follow.

APPENDIX C: COMPUTATION OF R_n^m WITH LARGE n

The $R_n^m(\rho)$ are polynomials in ρ of degree n, given explicitly as

$$R_n^m(\rho) = \sum_{s=0}^{p} \binom{n-s}{p}\binom{p}{s}(-1)^s \rho^{n-2s} \, , \tag{C1}$$

where $p = \frac{1}{2}(n-m)$. This explicit form is for some software awkward to use in computations for large n: when $m=0$, $n=40$, loss-of-digits occurs in 15 decimal places. For $m = 0, \ 1, \ \cdots$ fixed, and $M = 0, \ 1, \ \cdots$ fixed, the R_n^m can be computed for $n = m, \ m+2, \ \cdots, m+2M$ in the form of a DCT (Discrete Cosine Transform) as[35]

$$R_n^m(\rho) = \frac{1}{N}\sum_{k=0}^{N-1} U_n(\rho\cos\frac{2\pi k}{N})\cos\frac{2\pi m k}{N} \; , \;\; 0 \leq \rho \leq 1 \; , \tag{C2}$$

where U_n is the Chebyshev polynomial of degree n and of the second kind, and N is any integer $> 2(m+M)$.

[1] J.W.S. Rayleigh. *The Theory of Sound, Vol. 2, 1896.* (reprinted by Dover, New York), 1945.

[2] L.V. King. On the acoustic radiation field of the piezo-electric oscillator and the effect of viscosity on transmission. *Can. J. Res.*, 11:135–155, 1934.

[3] M. Greenspan. Piston radiator: Some extensions of the theory. *J. Acoust. Soc. Am.*, 65:608–621, 1979.

[4] G.R. Harris. Review of transient field theory for a baffled planar piston. *J. Acoust. Soc. Am.*, 70:10–20, 1981.

[5] R. New, R.I. Becker, and P. Wilhelmij. A limiting form for the nearfield of the baffled piston. *J. Acoust. Soc. Am.*, 70(5):1518-1526, 1981.

[6] T. Hasegawa, N. Inoue, and K. Matsuzawa. A new rigorous expansion for the velocity potential of a circular piston source. *J. Acoust. Soc. Am.*, 74(3):1044–1047, 1983.

[7] D.A. Hutchins, H.D. Mair, P.A. Puhach, and A.J. Osei. Continuous-wave pressure fields of ultrasonic transducers. *J. Acoust. Soc. Am.*, 80(1):1–12, 1986.

[8] R. C. Wittmann and A. D. Yaghjian. Spherical-wave expansions of piston-radiator fields. *J. Acoust. Soc. Am.*, 90(3):1647–1655, 1991.

[9] T. Hélie and X. Rodet. Radiation of a pulsating portion of a sphere: Application to horn radiation. *Acta Acustica united with Acustica*, 89(4), 565–577, 2003

[10] R.M. Aarts and A.J.E.M. Janssen. Approximation of the Struve function $\mathbf{H}_1$ occurring in impedance calculations. *J. Acoust. Soc. Am.*, 113(5):2635-2637, 2003.

[11] R.J. McGough, T.V. Samulski, and J.F. Kelly. An efficient grid sectoring method for calculations of the nearfield pressure generated by a circular piston. *J. Acoust. Soc. Am.*, 115(5):1942–1954, 2004.

[12] T.D. Mast and F. Yu. Simplified expansions for radiation from a baffled circular piston. *J. Acoust. Soc. Am.*, 118:3457–3464, 2005.

[13] T.J. Mellow. On the sound field of a resilient disk in an infinite baffle. *J. Acoust. Soc. Am.*, 120:90–101, 2006.

[14] J.F. Kelly and R.J. McGough. An annular superposition integral for axisymmetric radiators. *J. Acoust. Soc. Am.*, 121:759–765, 2007.

[15] Xiaozheng Zeng and R.J. McGough. Evaluation of the angular spectrum approach for simulations of near-field pressures. *J. Acoust. Soc. Am.*, 123(1):68–76, 2008.

[16] R.M. Aarts and A.J.E.M. Janssen. On-axis and far-field sound radiation from resilient flat and dome-shaped radiators. *J. Acoust. Soc. Am.*, 125(3):1444-1455, 2009.

[17] R.M. Aarts and A.J.E.M. Janssen. Sound radiation quantities arising from a resilient circular radiator. *J. Acoust. Soc. Am.*, 126(4):1776-1787, 2009.

[18] P.M. Morse and H. Feshbach. *Methods of theoretical physics.* McGraw-Hill, 1953.

[19] H. Stenzel and O. Brosze. *Guide to computation of sound phenomena (published in German as Leitfaden zur Berechnung von Schallvorgängen), 2nd ed.* Springer-Verlag, Berlin, 1958.

[20] P.M. Morse and K.U. Ingard. *Theoretical Acoustics.* McGraw-Hill Book Company, New York, 1968.

[21] E. Skudrzyk. *The Foundations of Acoustics.* Springer-Verlag, New York, 1971, ASA-reprint 2008.

[22] L.E. Kinsler, A.R. Frey, A.B. Coppens, and J.V. Sanders. *Fundamentals of Acoustics.* Wiley, New York, 1982.

[23] A.D. Pierce. *Acoustics, An Introduction to Its Physical Principles and Applications.* Acoustical Society of America through the American Institue of Physics, New York, 1989.

[24] D.T. Blackstock. *Fundamentals of Physical Acoustics.* John Wiley & Sons, New York, 2000.

[25] F.J.M. Frankort. *Vibration and Sound Radiation of Loudspeaker Cones.* Ph.D. dissertation, Delft University of Technology, 1975.

[26] A.J.E.M. Janssen and P. Dirksen. Concise formula for the Zernike coefficients of scaled pupils. *J. Microlith., Microfab., Microsyst.*, 5(3), 030501, July-Sept. 2006.

[27] A.J.E.M. Janssen, S. van Haver, P. Dirksen, and J.J.M. Braat. Zernike representation and Strehl ratio of optical systems with variable numerical aperture. *J. of Modern Optics*, 55(7), 1127–1157, 2008.

[28] L. Wright, S.P. Robinson, and V.F. Humphrey. Prediction of acoustic radiation from axisymmetric surfaces with arbitrary boundary conditions using the boundary element method on a distributed computing system. *J. Acoust. Soc. Am.*, 125:(3):1374-1383, 2009.

[29] M.J. Crocker (Ed.) *Handbook of Noise and Vibration Control.* Chapter 50: Use of Near-Field Acoustical Holography in Noise and Vibration Measurements, by E.G. Williams. J. Wiley Inc., New York, 2007.

[30] M. Abramowitz and I.A. Stegun. *Handbook of Mathematical Functions.* Dover, New York, 1972.

[31] A.B. Bhatia and E. Wolf. On the circle polynomials of Zernike and related orthogonal sets. *Proc. Camb. Phil. Soc.*, 50:40–48, 1954.

[32] M. Born and E. Wolf. *Principles of Optics*, 7th ed. Cambridge University Press, Cambridge, Chap. 9 and App. 7, 2002.

[33] A.J.E.M. Janssen and J.S.H. van Leeuwaarden. Relaxation time for the discrete D/G/1 queue. *Queueing Systems*, 50, 53-80, 2005.

[34] G. Szegö. *Orthogonal Polynomials.* AMS, Providence, 1939, 4th ed., 1975.

[35] A.J.E.M. Janssen and P. Dirksen. Computing Zernike polynomials of arbitrary degree using the discrete Fourier transform. *Journal of the European Optical Society - Rapid Publications*, 2, 07012, 2007.